Differential Ligand Recognition by the Src and Phosphatidylinositol 3-Kinase Src Homology 3 Domains: Circular Dichroism and Ultraviolet Resonance Raman Studies†

Nobuyuki Okishio,*,‡ Toshiyuki Tanaka,§ Ryuji Fukuda,‡ and Masako Nagai||

Department of Biochemistry, School of Medicine, Kanazawa University Faculty of Medicine, Kanazawa, Ishikawa 920-8640, Japan, Institute of Applied Biochemistry and Center for Tsukuba Advanced Research Alliance, University of Tsukuba, Tsukuba, Ibaraki 305-8572, Japan, and School of Health Sciences, Kanazawa University Faculty of Medicine, Kanazawa, Ishikawa 920-0942, Japan

Received July 16, 2002; Revised Manuscript Received October 11, 2002

ABSTRACT: Src homology 3 (SH3) domains recognize Pro-rich motifs using a hydrophobic cleft which contains several conserved aromatic residues. To investigate how aromatic residues contribute to ligand recognition, circular dichroism (CD) and 235 nm excited ultraviolet resonance Raman spectroscopies have been applied to Src and phosphatidylinositol 3-kinase (PI3K) SH3s. The CD analysis shows that Src SH3 binds to RPLPPLP (R-core) using aromatic residues with a dissociation constant (K_d) of 10 μM. Moreover, intensity increases of the Trp and Tyr Raman bands suggest that the interaction is mediated by hydrophobic contacts and/or hydrogen bond formation with both Trp and Tyr residues. In the interaction of Src SH3 with VSLARRPLPPLP (VSL12) (K_d 0.8 μM), Trp118 appears to form a strong hydrogen bond with VSL12, judging from significant intensity increases of the Trp Raman bands and the reported complex structure. In contrast, PI3K SH3 binds to R-core and VSL12 with lower affinities (K_d 34 and 18 μM, respectively), and the interactions are suggested to be mediated mainly by hydrophobic contacts and/or hydrogen bond formation with Tyr residue(s). In the D21N mutant (Asp21 → Asn) of PI3K SH3, whose hydrophobic cleft is deformed, Trp55 is shown to be responsible for the interaction with VSL12 by intensity increases of the Trp Raman bands. However, the affinity is severely decreased (K_d 330 μM). These observations imply that SH3 domains associate with their ligands with distinct use of aromatic residues and that hydrogen bond formation with an SH3-conserved Trp residue in the well-ordered hydrophobic cleft is important for stable complex formation.

Src homology 3 (SH3)[1] domains are found in various proteins involved in intracellular signal transduction and cytoskeletal organization and mediate inter- and intramolecular interactions (*1*). SH3 domains share among them a very similar β-barrel structure with a shallow groove on the protein surface which contains several highly conserved aromatic residues (usually one Trp and three Tyr or Phe) (*2*). This hydrophobic cleft plays a crucial role in binding with ligands, which typically contain a PxxP motif (x represents any amino acid residue) and adopt a polyproline type II (PPII) helix conformation (*2*). The PxxP motif is often flanked by a basic residue (usually Arg), which interacts with a conserved acidic residue in SH3 domains [Asp99 in Src SH3 and Asp21 in phosphatidylinositol 3-kinase (PI3K) SH3], and the positioning of this basic residue determines the binding orientation of ligands, which is categorized as class I or class II. The basic residue is located three residues N-terminal to the PxxP motif in class I ligands but is located two residues C-terminal to the motif in class II ligands (*3*−*6*).

The mechanism by which SH3 domains produce diversity and specificity for ligand recognition is one of the intriguing questions about SH3 domains. Although the hydrophobic cleft of SH3 domains provides an essential platform for the interaction with the PPII helix region of ligands, the maximal binding affinities of short Pro-rich peptides for SH3 domains are often low with dissociation constant (K_d) values in the range of 1−10 μM, and the relative differences in their affinities for different SH3 domains are not significant in many cases (*5*, *7*−*12*). On the other hand, molecular contacts outside both the hydrophobic cleft and the PPII helix region have been suggested to strengthen SH3−ligand interactions and provide specificity (*8*−*13*). The variable n-Src and RT loops of SH3 domains, which are adjacent to the hydrophobic

† This work was supported by a Grant-in-Aid for Scientific Research from the Ministry of Education, Science, Sports, and Culture of Japan to M.N. (14570103), a grant from the Honjin Foundation to N.O., and the Joint Studies Program (1999−2000) of the Institute for Molecular Science. T.T. is supported by JSPS and TARA.

* To whom correspondence should be addressed. Phone: +81 76 265 2176. Fax: +81 76 234 4225. E-mail: okishio@med.kanazawa-u.ac.jp.

‡ School of Medicine, Kanazawa University Faculty of Medicine.

§ University of Tsukuba.

|| School of Health Sciences, Kanazawa University Faculty of Medicine.

[1] Abbreviations: CD, circular dichroism; K_d, dissociation constant; PCR, polymerase chain reaction; PI3K, phosphatidylinositol 3-kinase; PPII, polyproline type II; SH3, Src homology 3; UVRR, ultraviolet resonance Raman.

10.1021/bi020475y CCC: $25.00
Published on Web 12/11/2002

cleft, are implied to be responsible for increased affinity and specificity for ligands.

However, is the hydrophobic cleft of SH3 domains really featureless in ligand recognition? To clarify how aromatic residues of SH3 domains specifically contribute to ligand recognition, we applied circular dichroism (CD) and 235 nm excited ultraviolet resonance Raman (UVRR) spectroscopies. CD spectroscopy in the UV region provides information on local environments of aromatic residues (*14*−*16*). On the other hand, 235 nm excited UVRR spectroscopy makes it possible to selectively observe vibrational spectra of Trp and Tyr residues (*17*), which can be used to probe their side-chain structures, environmental hydrophobicity and polarity, and hydrogen-bonding states (*17*−*20*).

In this study, we compared CD and UVRR spectral changes of Src and PI3K SH3s induced by two kinds of class I ligands, RPLPPLP (R-core) and VSLARRPLPPLP (VSL12) (*8*, *10*, *12*). Src and PI3K SH3s were selected because they are original and/or classical SH3 domains and their ligands are well characterized (*3*−*5*, *12*). In addition, we have extensively studied PI3K SH3 and its interaction with a class I ligand RKLPPRPSK (RLP1) by CD, UVRR, and nuclear magnetic resonance spectroscopies (*21*−*23*). The ligands R-core and VSL12 have the consensus SH3 binding sequence RPLPPΨP (Ψ stands for any hydrophobic amino acid residue), which was identified for Src, Fyn, Lyn, and PI3K SH3s by phage display techniques (*8*−*10*). Besides, VSL12, which was selected by Src SH3 as a peptide with a higher affinity than R-core (*10*), has an additional five residues (VSLAR) at the N-terminus of R-core. The results obtained in this study revealed that the hydrophobic clefts of Src and PI3K SH3s recognize these ligands in different ways. Also, we showed that the D21N mutation of PI3K SH3, which was found to deform the hydrophobic cleft (*21*, *22*), causes not only to decrease the binding affinities for the ligands but also to alter the interacting ways. These observations give insight into how SH3 domains form particular protein complexes necessary for precise signaling within cells.

MATERIALS AND METHODS

Sample Preparation. To express recombinant Src SH3, a pGEX6P-1 (Pharmacia Biotech) based expression plasmid was constructed as follows. The sequence encoding amino acid residues 82−140 of Src was amplified by polymerase chain reaction (PCR) using oligonucleotide primers (5′-cgg gat ccg gcg tca cca ctt tcg tgg ct-3′ and 5′-gga att ctc atc atc atg agg gcg cga cat agt tac t-3′) and pGEX-2T-Src SH3 (*24*, *25*) as a template. After digestion with *Bam*HI and *Eco*RI restriction endonucleases, the purified PCR-generated DNA fragment was subcloned into a pGEX6P-1 expression vector. The subcloned fragment was sequenced to confirm absence of mutations. The protein was expressed and purified in the similar way with recombinant PI3K SH3 and its D21N (Asp21 → Asn) mutant as described previously (*21*). These proteins include an additional five residues (GPLGS) from the vector sequence at the N-terminus of the domain, so that recombinant Src and PI3K SH3s consist of 64 and 90 amino acid residues, respectively. Protein concentrations were determined by absorbance at 280 nm. The extinction coefficients of proteins denatured in 6 M guanidine hydrochloride solution were calculated according to the method of Gill and von Hippel (*26*). The values are 16500 M^{-1} cm^{-1} for Src SH3 and 14650 M^{-1} cm^{-1} for PI3K SH3 and its D21N mutant. The purified synthetic peptides R-core (RPLPPLP-NH_2) and VSL12 (VSLARRPLPPLP-NH_2) were purchased from Sawady Technology (Tokyo, Japan). The peptide purity was certified to be more than 95% by the manufacturer.

CD Measurements and Determination of K_d Values. All CD spectra were recorded on a Jasco J-725 spectropolarimeter at 25 °C. The instrument was calibrated with *d*-10-camphorsulfonic acid. For each experiment, 20 spectra were obtained and averaged. CD data are expressed in terms of molar ellipticity [θ] (deg cm^2 $dmol^{-1}$). Determination of K_d values was performed by monitoring CD intensity change in the 220−230 nm region with increasing peptide concentrations as follows. Aliquots of a concentrated peptide solution (10 mM) were added to a solution of the domain (10 μM) in phosphate-buffered saline (8 mM Na_2HPO_4, 1.5 mM KH_2PO_4, 137 mM NaCl, 2.7 mM KCl, pH 7.4). The mixture was incubated at 25 °C in a stirred cell for 5−10 min before CD measurements. CD spectra were acquired at a scan speed of 100 nm min^{-1} with a 2 nm slit width and a 1 s response time. Light paths were 5 mm for Src and PI3K SH3s and 2 mm for the D21N mutant of PI3K SH3 to decrease absorbance in high peptide concentrations (500−1000 μM). The raw CD data were corrected for protein dilution and peptide CD intensity. K_d values were calculated by Scatchard analysis using the following equation where $\Delta[\theta]$ is the difference between the observed CD intensity and the CD intensity of the unliganded SH3 domain, $\Delta[\theta_\infty]$ denotes the difference between the CD intensity of the completely liganded SH3 domain and the CD intensity of the unliganded SH3 domain, [L] is the concentration of the free peptide, and n is the number of binding sites. The concentration of the free peptide was calculated by subtracting the concentration of the SH3−ligand complex, which was estimated by the CD intensity change, from the concentration of the added peptide.

$$(\Delta[\theta]/\Delta[\theta_\infty])/[\mathrm{L}] = n/K_d - (\Delta[\theta]/\Delta[\theta_\infty])/K_d$$

Other CD spectra were acquired for a light path of 1 mm at a scan speed of 50 nm min^{-1} with a 1 nm slit width and a 1 s response time. Sample concentration was 0.05 mM SH3 with or without 0.25 mM R-core or VSL12 (for the far-UV region: ca. 200−250 nm) or 0.2 mM SH3 with or without 1 mM R-core or VSL12 (for the near-UV region: ca. 250−300 nm) in 50 mM Tris-HCl (pH 7.2) containing 100 mM sodium sulfate. Sodium sulfate was used for an internal intensity standard in UVRR spectroscopy and, therefore, was added to CD samples to compare directly UVRR and CD data. Under the measurement condition, more than 95% (for 0.05 mM SH3) or 98% (for 0.2 mM SH3) of Src SH3, more than 85% (for 0.05 mM SH3) or 95% (for 0.2 mM SH3) of PI3K SH3, and ca. 30−40% (for 0.05 mM SH3) or ca. 60−70% (for 0.2 mM SH3) of the D21N mutant were estimated to be in the ligand-bound state on the basis of their K_d values.

UVRR Measurements. The 235 nm excited UVRR spectra were obtained with a XeCl excimer laser−pumped dye laser system (EMG103MSC/LPX120 and FL2002/SCANMATE, Lambda Physik) (*27*, *28*). The 308 nm line from a XeCl excimer laser (operated at 100 Hz) was used to excite

coumarin 480, and the 470 nm output from the dye laser was frequency-doubled with a β-BaB_2O_4 crystal to generate 235 nm pulses. The Raman excitation radiation (2−3 mJ cm^{-2}) was directed into the sample solution contained in a spinning cell from a lower front side. The scattered radiation was collected with Cassegrainian optics with *f*/1.1 and was dispersed with an asymmetric double monochromator (Spex 1404) in which the gratings in the first and second dispersion steps are 2400 (holographic) and 1200 grooves mm^{-1} (machine-ruled, 500 nm blaze), respectively. The Raman scattering was detected by an intensified photodiode array (PC-IMD/C5222-0110G; Hamamatsu Photonics). The temperature of a sample solution was kept at room temperature by flushing with cooled nitrogen gas against the cell. One spectrum is a sum of 400 exposures, each exposure accumulating the data for 0.8 s. The spinning cell was moved vertically by 1 mm to shift a laser illumination spot on the sample after each spectrum was acquired. The sample was replaced with a fresh one after eight spectra were obtained. A UVRR spectrum presented is a sum of 24−40 spectra. Raman shifts were calibrated with cyclohexane. Sample concentration was 0.2 mM SH3 with or without 1 mM R-core or VSL12 in 50 mM Tris-HCl (pH 7.2) containing 100 mM sodium sulfate. Under this condition, more than 98% of Src SH3, more than 95% of PI3K SH3, and ca. 60−70% of the D21N mutant were estimated to be in the ligand-bound state. The 982 cm^{-1} band of sulfate ions was used to normalize ordinate scales of spectra and to calculate differences. Intensity changes of Raman bands (percent) were calculated from peak intensity ratios.

RESULTS

Determination of K_d Values. We first assessed the binding affinities of Src and PI3K SH3s and the D21N mutant of PI3K SH3 for R-core and VSL12. On addition of R-core or VSL12 to the domain, the CD intensity in the 220−230 nm region increased with the peptide concentration, and these CD changes allowed one to determine the K_d value. In this study, the 220−230 nm region was selected to monitor CD intensity instead of the near-UV region (280−310 nm), which was used previously (*22*), because the near-UV spectral changes of the D21N mutant were too weak to estimate the binding affinity. The difference spectra of Src SH3 between with and without VSL12 at various ligand concentrations are depicted in Figure 1A as an example. The other difference spectra of the domains between with and without R-core or VSL12 at various ligand concentrations were similarly obtained. The largest CD difference in the 220−230 nm region (at 225 nm in Figure 1A) was plotted against the concentration of the added peptide (Figure 1B) and was used for Scatchard analysis (Figure 1C). The obtained K_d values are summarized in Table 1 (for binding parameters, see Supporting Information). The K_d values of Src SH3 for R-core and VSL12 were 10 and 0.8 μM, and those of PI3K SH3 were 34 and 18 μM, respectively. These values agree well with those reported previously by Rickles et al. (*10*) and Feng et al. (*12*) (Table 1). Src SH3 showed higher affinities for both R-core and VSL12 than PI3K SH3. In the D21N mutant, the affinities for R-core and VSL12 were severely decreased (500 and 330 μM, respectively), as was observed for RLP1 (460 μM) (*5*).

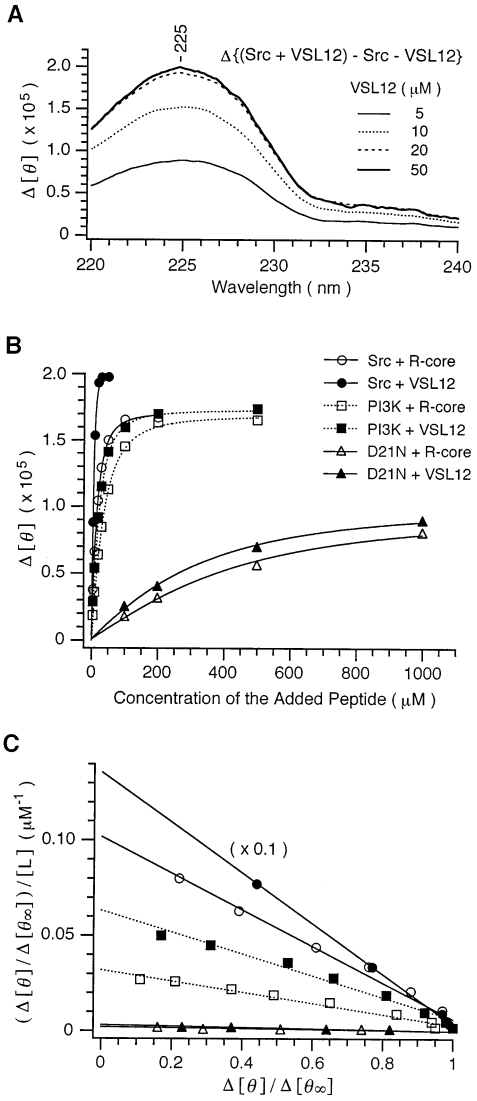

FIGURE 1: Binding assay of Src and PI3K SH3s and the D21N mutant of PI3K SH3 for R-core and VSL12. (A) Effect of the VSL12 binding on the UV CD difference spectra of Src SH3. The difference spectra between with and without VSL12 at various peptide concentrations are shown. (B) Titration curves of the largest CD differences in the 220−230 nm region between with and without R-core or VSL12 ($\Delta[\theta]$) of Src and PI3K SH3s and the D21N mutant of PI3K SH3. The largest CD difference is plotted against the concentration of the added peptide. (C) Scatchard analysis of the binding of R-core and VSL12 to Src and PI3K SH3s and the D21N mutant of PI3K SH3. The K_d value was calculated from the slope of the plot. In the Src SH3−VSL12 complex, 0.1 times the values of $(\Delta[\theta]/\Delta[\theta_\infty])/[L]$ are plotted. The values of slope, the coefficients of determination (r^2), and the numbers of binding sites (n) are summarized in Table S1 of Supporting Information.

CD Analysis of Src and PI3K SH3s. CD bands in the near-UV region are generally dominated by contributions from aromatic side chains and disulfides (*14*−*16*). Src SH3 contains four Tyr (Tyr90, Tyr92, Tyr131, and Tyr136), two Trp (Trp118 and Trp119), two Phe (Phe86 and Phe102), and no Cys residues. PI3K SH3 has seven Tyr (Tyr6, Tyr8, Tyr12, Tyr14, Tyr59, Tyr73, and Tyr76), one Trp (Trp55), two Phe (Phe42 and Phe69), and no Cys residues. Since R-core and VSL12 contain neither aromatic nor Cys residues, the near-UV CD changes of Src and PI3K SH3s by the ligand addition are attributed to the local environmental changes of these aromatic side chains upon ligand association.

Table 1: Dissociation Constants of Src and PI3K SH3s and the D21N Mutant of PI3K SH3 for R-core and VSL12

		K_d (μM)		
SH3 domain	peptide	Okishio et al.[a]	Rickles et al.[b]	Feng et al.[c]
Src	R-core	10	17.7	3.7
	VSL12	0.8	0.86	0.45
PI3K	R-core	34	38.8	20
	VSL12	18	14.9	12
D21N	R-core	500		
	VSL12	330		

[a] Determined in this work by CD measurements using RPLPPLP-NH_2 (R-core) or VSLARRPLPPLP-NH_2 (VSL12). [b] Determined by fluorescence measurements using Ac-RPLPPLPGGK-NH_2 (Ac-R-core + GGK) or Ac-VSLARRPLPPLPGGK-NH_2 (Ac-VSL12 + GGK) (*10*). [c] Determined by fluorescence measurements using Ac-RPLPPLP-NH_2 (Ac-R-core) or Ac-VSLARRPLPPLP-NH_2 (Ac-VSL12) (*12*).

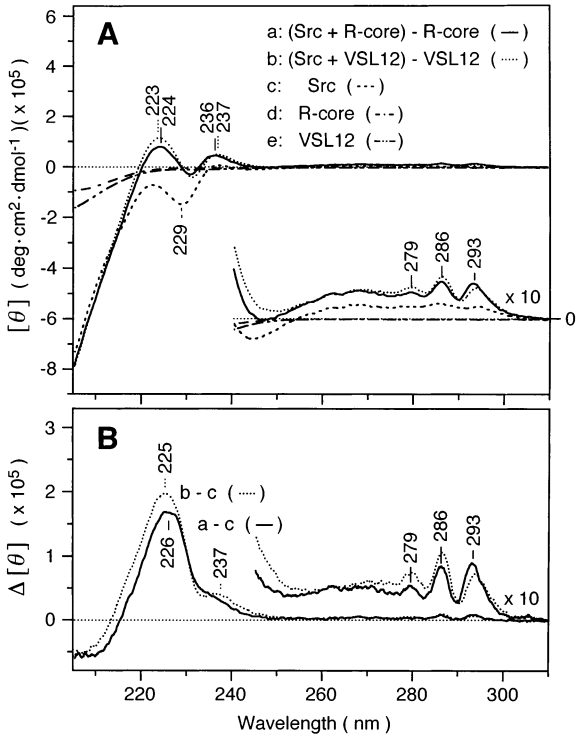

FIGURE 2: UV CD spectra of Src SH3 with and without R-core or VSL12 (A) and the difference spectra (B). The spectra of free R-core and VSL12 were also drawn in (A) and were subtracted from those of the SH3−ligand mixture. The sample concentration was 0.05 mM SH3 with or without 0.25 mM peptide (0.2 mM SH3 with or without 1 mM peptide for 10-fold expanded spectra in the near-UV region) in 50 mM Tris-HCl buffer (pH 7.2) containing 100 mM sodium sulfate.

Figure 2A shows the UV CD spectra of Src SH3 with and without R-core or VSL12. The addition of R-core and VSL12 to Src SH3 resulted in distinct spectral changes in both the near- and far-UV regions. The difference spectra showed peaks at 293, 286, 279, and 226 nm for R-core and at 293, 286, 279, 237, and 225 nm for VSL12 (Figure 2B). VSL12 caused larger intensity changes than R-core for all peaks except one at 293 nm. The observed spectral differences are not due to the difference in binding affinities, because under the measurement condition, more than 95% (for 0.05 mM SH3) or 98% (for 0.2 mM SH3) of Src SH3 was estimated to be in the ligand-bound state.

Figure 3A shows the UV CD spectra of PI3K SH3 with and without R-core or VSL12. The addition of R-core and

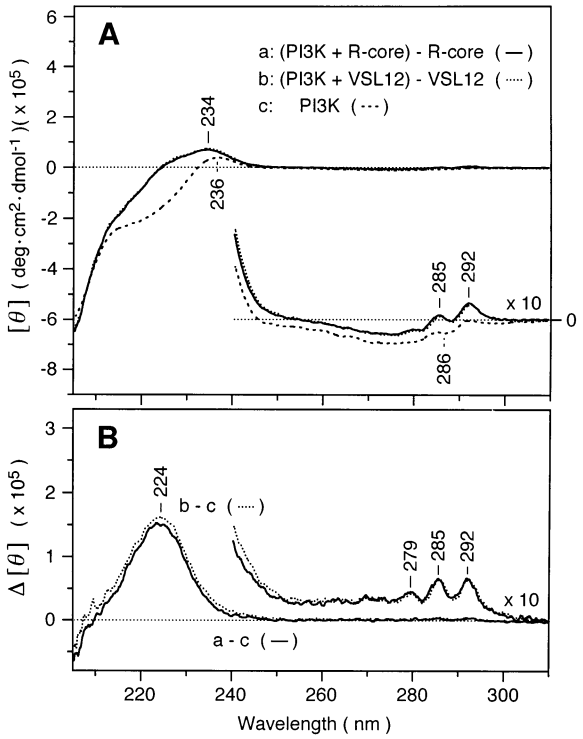

FIGURE 3: UV CD spectra of PI3K SH3 with and without R-core or VSL12 (A) and the difference spectra (B). The spectra of free R-core and VSL12 were subtracted from those of the SH3−ligand mixture. Experimental conditions were the same as those in Figure 2.

VSL12 to PI3K SH3 caused spectral changes similar to each other, and the difference spectra showed peaks at 292, 285, 279, and 224 nm (Figure 3B).

UVRR Analysis of Src and PI3K SH3s. The environmental and structural changes in Src and PI3K SH3s induced by R-core and VSL12 were further examined using 235 nm excited UVRR spectroscopy. At this excitation wavelength, a strong enhancement is expected for the vibrational modes associated with Trp and Tyr residues (*17*). Since R-core and VSL12 have no aromatic residues, these peptides showed only the 982 cm^{-1} band of sulfate ions (Figure 4F,G). Therefore, 235 nm excited UVRR spectroscopy was able to selectively monitor the changes of Trp and Tyr residues in the SH3 domains.

As shown in Figure 4C, Raman bands of Src SH3 were seen at 1208 (Y7a), 1177 (Y9a), 1011 (W16), 876 (W17), 855 and 830 (Tyr doublet, Y1 and 2 × Y16a), and 762 cm^{-1} (W18). The R-core addition brought about characteristic changes in these Raman bands (Figure 4A,D): intensity increments of W16 (ca. 5%), W17 (ca. 5%), W18 (ca. 10%), Y7a (ca. 10%), Y9a (ca. 10%), and Tyr doublet (ca. 10−15%). On the other hand, the VSL12 addition caused spectral changes distinct from those induced by the R-core addition (Figure 4B,E). The intensity increments of Trp Raman bands were prominent (W16, ca. 20%; W17, ca. 20%; W18, ca. 30%), while the spectral changes of Tyr Raman bands were obscure. It should be noted that the difference spectrum had two positive peaks at 880 and 870 cm^{-1} in the W17 region (Figure 4E).

As for PI3K SH3, Raman bands were seen at 1208 (Y7a), 1173 (Y9a), 1010 (W16), 854 and 830 (Tyr doublet, Y1 and 2 × Y16a), and 759 cm^{-1} (W18) (Figure 5C). The W17 band

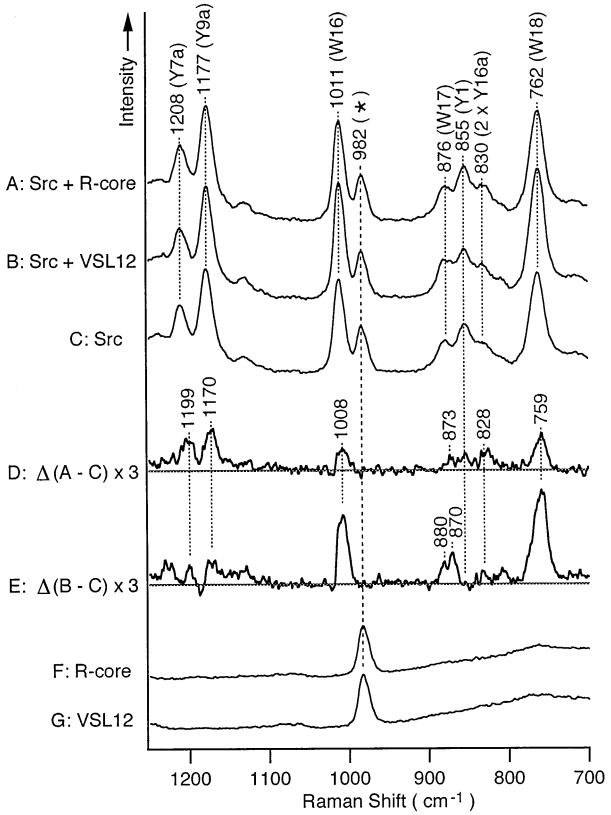

FIGURE 4: 235 nm excited UVRR spectra of Src SH3 with R-core (A) or VSL12 (B) and without a peptide (C) and the 3-fold difference spectra (D and E). The spectra of free R-core and VSL12 are also shown (F and G, respectively). The Raman bands of Trp and Tyr vibrations are labeled by W and Y, respectively, with their mode designations established by Harada and Takeuchi (*19*). For example, W16 is the symmetric benzene/pyrrole out-of-phase breathing mode of Trp. The asterisk denotes the Raman band of sulfate ions (982 cm^{-1}) used as an internal intensity standard. The sample concentration was 0.2 mM SH3 with or without 1 mM peptide in 50 mM Tris-HCl buffer (pH 7.2) containing 100 mM sodium sulfate.

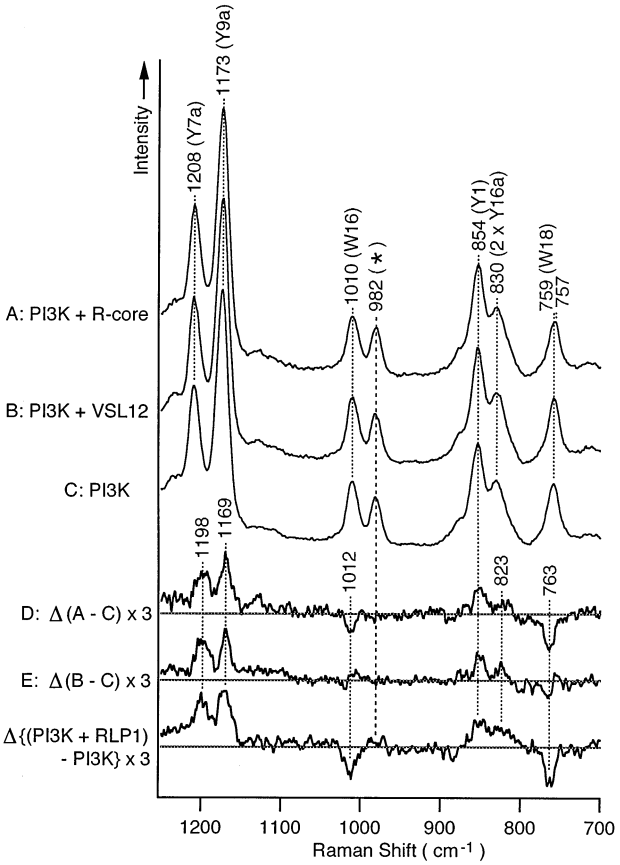

FIGURE 5: 235 nm excited UVRR spectra of PI3K SH3 with R-core (A) or VSL12 (B) and without a peptide (C) and the 3-fold difference spectra (D and E). Experimental conditions were the same as those in Figure 4. The difference spectrum of PI3K SH3 (0.2 mM) between with and without RLP1 (0.8 mM) (F) was reported previously (*23*).

was not clearly seen in PI3K SH3 because of the overlap with the strong Tyr doublet band. The R-core addition caused intensity decrements of W16 (ca. 10%) and W18 (ca. 15%), intensity increments of Y7a (ca. 5%), Y9a (ca. 5%), and Tyr doublet (ca. 5%), and a frequency downshift by 2 cm^{-1} of W18 (Figure 5A,D). These spectral changes resemble those induced by RLP1 (Figure 5F) (*21*, *23*). The VSL12 addition caused similar spectral changes in Tyr Raman bands with the R-core addition (Figure 5B,E). However, intensity changes of Trp Raman bands and a shift of the W18 frequency, which is sensitive to a hydrogen-bonding state (*29*), were not clear in the case of the VSL12 addition (Figure 5B,E).

The D21N Mutant of PI3K SH3. We previously demonstrated that the D21N mutation of PI3K SH3 causes to deform the ligand binding cleft, decrease the binding affinity for RLP1, and alter the RLP1 interacting way (*21*, *22*). Therefore, effects of the D21N mutation on the recognition of R-core and VSL12 were examined. Figure 6A shows the UV CD spectra of the D21N mutant with and without R-core or VSL12. The difference spectra showed just a small peak at 226 nm (Figure 6B).

The D21N mutant was further subjected to the UVRR analysis (Figure 7). The R-core addition did not induce any

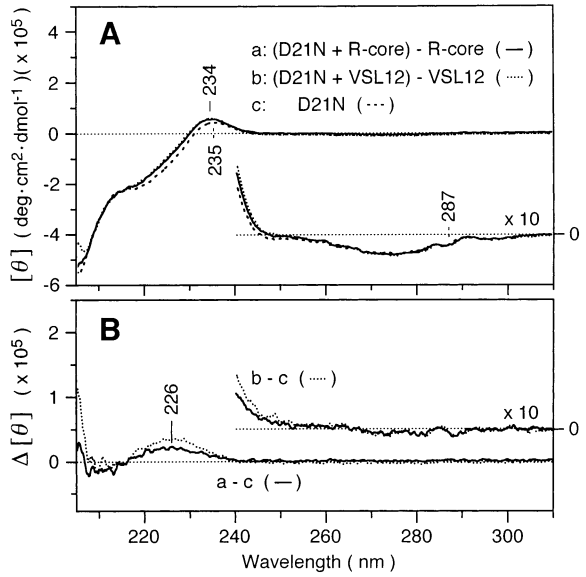

FIGURE 6: UV CD spectra of the D21N mutant of PI3K SH3 with and without R-core or VSL12 (A) and the difference spectra (B). The spectra of free R-core and VSL12 were subtracted from those of the SH3−ligand mixture. Experimental conditions were the same as those in Figure 2.

remarkable spectral changes (Figure 7A,E). In contrast, prominent changes were observed upon the VSL12 addition: intensity increments of W16 (ca. 15%), W18 (ca. 20%),

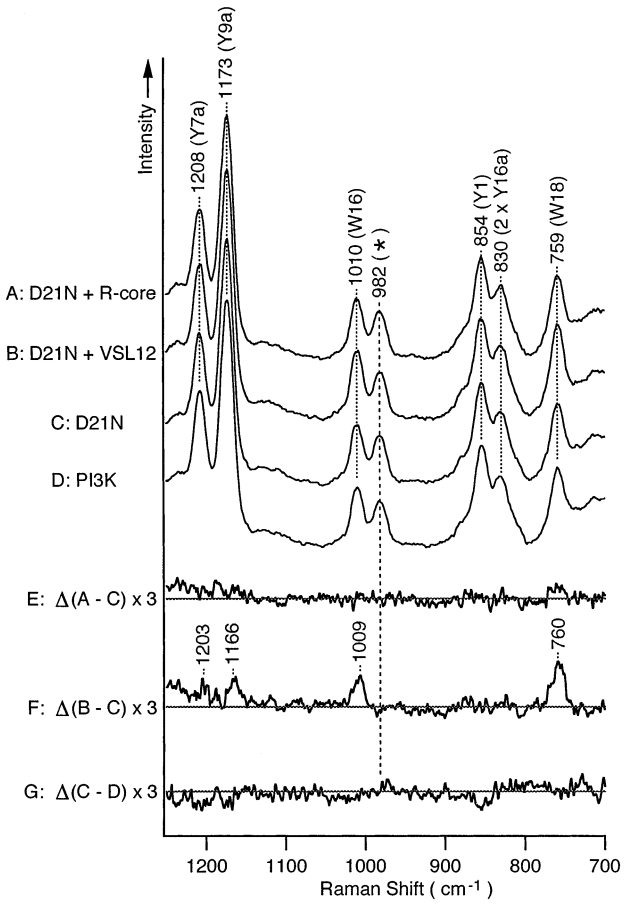

FIGURE 7: 235 nm excited UVRR spectra of the D21N mutant of PI3K SH3 with R-core (A) or VSL12 (B) and without a peptide (C) and the 3-fold difference spectra (E and F). The spectrum of wild-type PI3K SH3 (D) and the 3-fold difference spectrum between the D21N mutant and the wild type (G) are also shown. Experimental conditions were the same as those in Figure 4.

Y7a (ca. 2%), and Y9a (ca. 2%) (Figure 7B,F). There were no discernible differences between the wild type and the D21N mutant before peptide addition (Figure 7C,D,G).

DISCUSSION

CD and UVRR Analyses of Src SH3. The interactions with R-core and VSL12 brought about distinct CD spectral changes in Src SH3 (Figure 2). This indicates that these ligands induce different kinds of environmental and/or structural changes in the aromatic side chains of Src SH3; in other words, these ligands bind to the domain in different ways. This is also supported by the UVRR analysis shown in Figure 4; the intensity increments of Trp Raman bands by VSL12 are larger than those by R-core (Figure 4D,E), and the difference spectrum between with and without VSL12 gives two distinct positive peaks in the W17 region (Figure 4E), which must be derived from Trp118 and Trp119. These results denote that the VSL12 binding causes both Trp118 and Trp119 to be placed in a much more hydrophobic environment than the R-core binding and that their indole NH sites may be strongly hydrogen bonded in the VSL12-bound form (*29*−*31*).

The interactions with R-core and VSL12 also induced distinct changes in Tyr Raman bands; the R-core binding caused intensity increments of Tyr Raman bands (Figure 4D), whereas their intensity changes were obscure in the VSL12-bound form (Figure 4E). One possible reason is that Tyr residue(s) is (are) placed in a more hydrophobic environment and its (their) phenolic OH group(s) is (are) hydrogen bonded by the association with R-core but not with VSL12 (*31*, *32*). Another is that Tyr residue(s) is (are) placed in a more hydrophobic environment and is (are) hydrogen bonded in the VSL12-bound form, but some other Tyr residue(s) is (are) coincidently transferred to be in a more hydrophilic (more polar) environment possibly with its (their) hydrogen bonding reduced or depleted. The latter case seems more plausible, judging from the reported complex structure of Src SH3 with VSL12 (*12*). Anyhow, these changes are likely to be derived from direct intermolecular interactions, because every Tyr residue of Src SH3 is located in the hydrophobic cleft (*4*, *12*, *24*).

CD and UVRR Analyses of PI3K SH3 and Its D21N Mutant. In PI3K SH3, the addition of R-core and VSL12 induced similar spectral changes in UV CD (Figure 3) and Tyr Raman bands (Figure 5D,E). The intensity increments of Tyr Raman bands indicate that Tyr residue(s) is (are) placed in a more hydrophobic environment and may be hydrogen bonded (*31*, *32*). On the other hand, intensity changes of Trp Raman bands and a frequency shift of W18 were not clear in the VSL12-bound form (Figure 5B,E). This denotes that Trp55 is transferred to be in a more hydrophilic (more polar) environment and its hydrogen bonding is reduced or depleted by the association with R-core but not with VSL12 (*29*, *31*).

The UVRR spectral changes of PI3K SH3 by R-core resemble those by RLP1 in both Trp and Tyr Raman bands (Figure 5D,F). Besides, R-core and RLP1 share a similar amino acid sequence (RPLPPLP and RKLPPRPSK, where identical amino acid residues are underlined), and they bind to PI3K SH3 with similar affinities (K_d 34 and 19 μM, respectively) (*22*). Therefore, R-core and RLP1 may interact with PI3K SH3 in a similar way. In the previous study, we demonstrated that Tyr14 is a main contributor to the spectral changes of Tyr Raman bands by RLP1 (*23*). Likewise, Tyr14 may be responsible for the spectral changes by R-core. Although the affected Tyr residue(s) by VSL12 has (have) not been assigned, such conserved Tyr residues as Tyr12, Tyr14, and Tyr73, which constitute the hydrophobic cleft (*5*, *33*−*35*), are highly possible.

In the D21N mutant of PI3K SH3, the affinities for R-core and VSL12 were severely decreased (Table 1), and the CD spectral changes induced by these peptides were very weak (Figure 6). However, an interesting feature was observed in the UVRR analysis; the intensities of Trp Raman bands were remarkably increased by the VSL12 addition (Figure 7F). This indicates that Trp55 is placed in a more hydrophobic environment and may be hydrogen bonded (*29*−*31*). These changes are totally different from those observed in the wild-type PI3K SH3 (Figure 5E) but rather similar to those in Src SH3 (Figure 4E).

Difference in Ligand Interaction between Src and PI3K SH3s. Src and PI3K SH3s have positive bands above 290 nm in the CD difference spectra (Figures 2B and 3B). This result may reflect their similarity in the perturbation of Trp residue(s) by the ligand addition. However, the UVRR analysis showed that environmental and structural changes of Trp residue(s) are different between Src and PI3K SH3s. In Src SH3, Trp118 and/or Trp119 for the R-core binding

and both Trp118 and Trp119 for the VSL12 binding are placed in a more hydrophobic environment and may be hydrogen bonded. In PI3K SH3, Trp55 is placed in a more hydrophilic (more polar) environment, and its hydrogen bonding is reduced or depleted only by the R-core binding. The discrepancy between the CD and UVRR results may be due to differences in the information obtained from CD and UVRR spectroscopies. Generally, it is difficult to specify the factors generating CD differences (*16*). In addition, the responsible Trp residue(s) for the CD changes has (have) not been assigned for Src SH3. Therefore, the similarity in CD changes between Src and PI3K SH3s was not taken into consideration for model construction (see below).

In Src and PI3K SH3s, Tyr residue(s) appears (appear) to be placed in a more hydrophobic environment and may be hydrogen bonded by the interactions with R-core and VSL12. However, there is a distinct difference in the Tyr doublet between Src and PI3K SH3s. For Src SH3, the 828 cm^{-1} line increases with the ligand binding (Figure 4D,E), while for PI3K SH3, it is the 854 cm^{-1} line that is enhanced (Figure 5D,E). The intensity ratio of the Tyr doublet (I_{850}/I_{830}) is a good indicator to know whether Tyr residue(s) is (are) exposed or buried (*18*): when the ratio is high, it is interpreted that Tyr residue(s) is (are) exposed. Therefore, the results obtained suggest that Tyr residue(s) of Src SH3 may be more buried than that (those) of PI3K SH3 when complexed with the ligands.

SH3−Ligand Interactions through Trp Residues. The addition of R-core and VSL12 induced different environmental and structural changes of Trp and Tyr residues in Src and PI3K SH3s and the D21N mutant of PI3K SH3. Particularly, the changes of Trp residues were shown to be distinct and prominent by the UVRR analysis. Figure 8 shows models of the possible SH3−ligand interactions through Trp residues on the basis of our results and the reported complex structure of Src SH3 with RALPPLPRY (RLP2) (*4*) or VSL12 (*12*) and that of PI3K SH3 with RLP1 (*5*). In Src SH3 (Figure 8A), on the analogy of the complex structure of Src SH3−RLP2, the indole NH of Trp118, a conserved Trp residue, is likely to be close to the main-chain carbonyl group of Arg1 of R-core, and there may be a hydrogen bond. Trp118 is also reported to form a hydrogen bond with Arg6 of VSL12 (*12*). Our UVRR results (Figure 4D,E) suggest that the hydrogen bond with Arg1 of R-core, even if it exists, may be weaker than that with Arg6 of VSL12. On the other hand, Trp119, a nonconserved Trp residue, appears not to directly interact with R-core or VSL12. The indole NH of Trp119 is close to the main-chain carbonyl group of Gly116 in the RLP2-bound form and those of Asn113, Gly116, and Asp117 in the VSL12-bound form. Therefore, the environmental and structural changes of Trp119 are thought to arise from the intramolecular interactions accompanied by the ligand association.

In PI3K SH3 (Figure 8B), on the analogy of the complex structure of PI3K SH3−RLP1, Trp55, a conserved Trp residue, may be surrounded by the main-chain amino and side-chain guanidino groups of Arg1 and the main-chain amide group of Leu3 of R-core. The binding mode of VSL12 may resemble that of R-core, judging from the similarity in CD difference spectra (Figure 3B). However, our UVRR results (Figure 5D,E) suggest that Trp55 may be less surrounded by such groups as the side-chain guanidino group

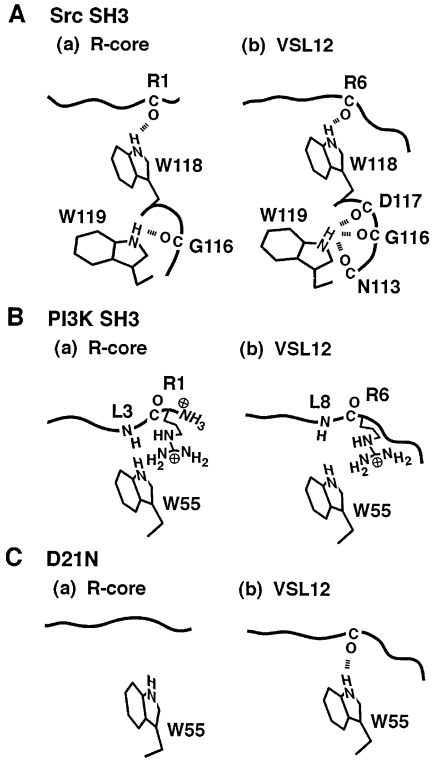

FIGURE 8: Models showing possible interactions of Src and PI3K SH3s and the D21N mutant of PI3K SH3 with R-core or VSL12 through Trp residues (A, B, and C, respectively). (A) The side chains of Trp118 and Trp119 and a part of the C_α backbone trace of Src SH3 are depicted with a part of the C_α backbone trace of R-core or VSL12. (B) The side chain of Trp55 of PI3K SH3 and that of Arg1 of R-core or Arg6 of VSL12 are depicted with a part of the C_α backbone trace of R-core or VSL12. (C) The side chain of Trp55 of the D21N mutant is depicted with a part of the C_α backbone trace of R-core or VSL12.

of Arg6 and the main-chain amide group of Leu8 of VSL12. In the D21N mutant (Figure 8C), the interaction with R-core is very weak. However, Trp55 may form a hydrogen bond with VSL12 (Figure 7F).

Factors for Stable SH3−Ligand Complex Formation. The environmental and structural changes of Trp residues are different not only among the domains but also between the ligands (Figure 8). In the Src SH3−VSL12 complex, the hydrogen bond formation between Trp118 and VSL12 seems to be essential for stable complex formation. VSL12 has an additional five residues (VSLAR) at the N-terminus of R-core, and the first six residues (VSLARR) of VSL12 are reported to contact a large pocket formed by the n-Src and RT loops of Src SH3 (*12*). Our results suggest that the VSLAR sequence may increase the affinity by not only interacting with Src SH3 outside the hydrophobic cleft but also assisting the ligand to settle in an optimal position to form a hydrogen bond with Trp118. The latter function seems more important for the tight interaction, because a peptide having only the flank sequence does not bind to Src SH3 (*12*).

In some SH3 domains, hydrogen bond formation between an SH3-conserved Trp residue and a ligand backbone may be indispensable for stable SH3−ligand complex formation. In the complex structure of Src SH3 with VSL12 (*12*) and that of Abl SH3 with the 3BP-1 peptide (APTMPPPLPP) (*36*) or its derivative p41 (APSYSPPPPP) (*37*), all of which

are class I ligands, the distance between the $N_{\epsilon 1}$ atom of the conserved Trp residue and the closest main-chain carbonyl oxygen of the ligand is approximately 3 Å, indicating the presence of a hydrogen bond. In contrast, the distance is about 6 Å in PI3K SH3−RLP1 (*5*). The capability of the hydrogen bond formation can be one of the influential factors for binding affinity. For Src and Abl SH3s, two short Pro-rich peptides that possess a K_d value less than 1 μM have been already reported: VSL12 for Src SH3 (K_d 0.45−0.86 μM) (*10*, *12*) and p40 (APTYSPPPPP), a derivative of the 3BP-1 peptide, for Abl SH3 (K_d 0.4 μM) (*38*). However, such a peptide has not yet been reported for PI3K SH3. The lowest K_d value for PI3K SH3 is 7.6 μM, which was determined with RKLPPRPRR, a composite of class I and II ligands (*3*). There must be such structural factors as restraining Trp55 from forming a hydrogen bond with a ligand. One possible factor is the position of Asp21, which may interact with Arg1 of R-core or Arg6 of VSL12 and determine the location of the residue. This structural restraint is expected to be loosened in the D21N mutant, so that Trp55 may form a hydrogen bond in a hydrophobic environment with VSL12, as is suggested by the UVRR analysis (Figure 7F).

Despite a possible hydrogen bond with Trp55, the affinity of the D21N mutant for VSL12 was severely decreased (Table 1). In the D21N mutant, the electrostatic interaction via Asp21 is lost (*5*), and its hydrophobic cleft is deformed (*21*, *22*). These facts suggest that hydrogen bond formation between an SH3-conserved Trp residue and a ligand backbone may contribute well to stable SH3−ligand complex formation only in the context of the well-ordered hydrophobic cleft.

Modulation of SH3−Ligand Interactions. In this study, we showed that the interactions with R-core and VSL12 induced different environmental and structural changes in Src and PI3K SH3s and the D21N mutant of PI3K SH3. This suggests that ligands of SH3 domains may take variable conformations depending on binding partners, and resultant SH3−ligand complex structures can be divergent despite the similarities in their binding affinities. Recently, Briggs et al. (*39*) reported interesting results using the coexpression system of Nef, a human immunodeficiency virus accessory protein, with a tyrosine kinase of the Src family, Hck or Lyn; the coexpression of Nef with Hck brought about the activation of Hck, whereas the coexpression of Nef with Lyn showed no effect on the activity of Lyn. Nef is suggested to bind to the SH3 domain of Hck and activate it. In addition, Hck and Lyn are highly homologous (ca. 70% identities in the SH3 domains as well as the entire amino acid sequences) and interact with Nef with similar affinities (*39*, *40*). Therefore, the distinct results of the coexpression experiments may be due to the differences in the complex structures of Nef-Hck SH3 and Nef-Lyn SH3. This kind of modulation of SH3−ligand interactions is thought to be indispensable for SH3-mediated signaling, so that ligands of SH3 domains can exert various effects depending on binding partners.

So far, the following scheme is widely accepted for SH3−ligand interactions; the hydrophobic cleft recognizes a common core of the PPII helix region, while the n-Src and RT loops undertake fine control of specificity. However, our study clearly showed that the hydrophobic cleft not only provides a basic platform for the interaction with the PPII helix region but also plays an important role in producing diversity and specificity for ligand recognition by modulating SH3−ligand interactions. Also, our observation on the importance of hydrogen bond formation with an SH3-conserved Trp residue for stable SH3−ligand complex formation gives basal knowledge for rational design of high-affinity ligands toward artificial control of intracellular signaling via SH3 domains.

ACKNOWLEDGMENT

We thank Professor Teizo Kitagawa and Dr. Shigenori Nagatomo for use of UVRR equipment and helpful suggestions for preparing the manuscript and Professor Stuart L. Schreiber and Dr. Hongtao Yu for providing the pGEX-2T-Src SH3 expression plasmid and the PI3K SH3-RLP1 coordinates prior to PDB release.

SUPPORTING INFORMATION AVAILABLE

Table S1 showing several parameters used to determine the K_d values of Src and PI3K SH3s and the D21N mutant of PI3K SH3 for R-core and VSL12. This material is available free of charge via the Internet at http://pubs.acs.org.

REFERENCES

1. Pawson, T. (1995) *Nature 373*, 573−580.
2. Lee, C.-H., Cowburn, D., and Kuriyan, J. (1998) *Methods Mol. Biol. 84*, 3−31.
3. Chen, J. K., Lane, W. S., Brauer, A. W., Tanaka, A., and Schreiber, S. L. (1993) *J. Am. Chem. Soc. 115*, 12591−12592.
4. Feng, S., Chen, J. K., Yu, H., Simon, J. A., and Schreiber, S. L. (1994) *Science 266*, 1241−1247.
5. Yu, H., Chen, J. K., Feng, S., Dalgarno, D. C., Brauer, A. W., and Schreiber, S. L. (1994) *Cell 76*, 933−945.
6. Lim, W. A., Richards, F. M., and Fox, R. O. (1994) *Nature 372*, 375−379.
7. Viguera, A. R., Arrondo, J. L. R., Musacchio, A., Saraste, M., and Serrano, L. (1994) *Biochemistry 33*, 10925−10933.
8. Sparks, A. B., Quilliam, L. A., Thorn, J. M., Der, C. J., and Kay, B. K. (1994) *J. Biol. Chem. 269*, 23853−23856.
9. Rickles, R. J., Botfield, M. C., Weng, Z., Taylor, J. A., Green, O. M., Brugge, J. S., and Zoller, M. J. (1994) *EMBO J. 13*, 5598−5604.
10. Rickles, R. J., Botfield, M. C., Zhou, X.-M., Henry, P. A., Brugge, J. S., and Zoller, M. J. (1995) *Proc. Natl. Acad. Sci. U.S.A. 92*, 10909−10913.
11. Sparks, A. B., Rider, J. E., Hoffman, N. G., Fowlkes, D. M., Quilliam, L. A., and Kay, B. K. (1996) *Proc. Natl. Acad. Sci. U.S.A. 93*, 1540−1544.
12. Feng, S., Kasahara, C., Rickles, R. J., and Schreiber, S. L. (1995) *Proc. Natl. Acad. Sci. U.S.A. 92*, 12408−12415.
13. Lee C.-H., Leung, B., Lemmon, M. A., Zheng, J., Cowburn, D., Kuriyan, J., and Saksela, K. (1995) *EMBO J. 14*, 5006−5015.
14. Strickland, E. H. (1974) *CRC Crit. Rev. Biochem. 2*, 113−175.
15. Woody, R. W. (1995) *Methods Enzymol. 246*, 34−71.
16. Kelly, S. M., and Price, N. C. (1997) *Biochim. Biophys. Acta 1338*, 161−185.
17. Kitagawa, T., and Hirota, S. (2002) in *Handbook of Vibrational Spectroscopy* (Chalmers, J. M., and Griffiths, P. R., Eds.) Vol. 5, pp 3426−3446, John Wiley & Sons Ltd., Chichester.
18. Tu, A. T. (1986) in *Spectroscopy of Biological Systems* (Clark, R. J. H., and Hester, R. E., Eds.) pp 47−112, John Wiley & Sons Ltd., Chichester.
19. Harada, I., and Takeuchi, H. (1986) in *Spectroscopy of Biological Systems* (Clark, R. J. H., and Hester, R. E., Eds.) pp 113−175, John Wiley & Sons Ltd., Chichester.
20. Austin, J. C., Rodgers, K. R., and Spiro, T. G. (1993) *Methods Enzymol. 226*, 374−396.
21. Okishio, N., Nagai, M., Fukuda, R., Nagatomo, S., and Kitagawa, T. (2000) *Biopolymers 57*, 208−217.
22. Okishio, N., Tanaka, T., Fukuda, R., and Nagai, M. (2001) *Biochemistry 40*, 119−129.

23. Okishio, N., Tanaka, T., Nagai, M., Fukuda, R., Nagatomo, S., and Kitagawa, T. (2001) *Biochemistry 40*, 15797−15804.
24. Yu, H., Rosen, M. K., Shin, T. B., Seidel-Dugan, C., Brugge, J. S., and Schreiber, S. L. (1992) *Science 258*, 1665−1668.
25. Yu, H., Rosen, M. K., and Schreiber, S. L. (1993) *FEBS Lett. 324*, 87−92.
26. Gill, S. C., and von Hippel, P. H. (1989) *Anal. Biochem. 182*, 319−326.
27. Kaminaka, S., and Kitagawa, T. (1992) *Appl. Spectrosc. 46*, 1804−1808.
28. Nagatomo, S., Nagai, M., Tsuneshige, A., Yonetani, T., and Kitagawa, T. (1999) *Biochemistry 38*, 9659−9666.
29. Matsuno, M., and Takeuchi, H. (1998) *Bull. Chem. Soc. Jpn. 71*, 851−857.
30. Hu, X., and Spiro, T. G. (1997) *Biochemistry 36*, 15701−15712.
31. Chi, Z., and Asher, S. A. (1998) *J. Phys. Chem. B 102*, 9595−9602.
32. Hashimoto, S., Yabusaki, T., Takeuchi, H., and Harada, I. (1995) *Biospectroscopy 1*, 375−385.
33. Koyama, S., Yu, H., Dalgarno, D. C., Shin, T. B., Zydowsky, L. D., and Schreiber, S. L. (1993) *Cell 72*, 945−952.
34. Booker, G. W., Gout, I., Downing, A. K., Driscoll, P. C., Boyd, J., Waterfield, M. D., and Campbell, I. D. (1993) *Cell 73*, 813−822.
35. Liang, J., Chen, J. K., Schreiber, S. L., and Clardy, J. (1996) *J. Mol. Biol. 257*, 632−643.
36. Musacchio, A., Saraste, M., and Wilmanns, M. (1994) *Nat. Struct. Biol. 1*, 546−551.
37. Pisabarro, M. T., Serrano, L., and Wilmanns, M. (1998) *J. Mol. Biol. 281*, 513−521.
38. Pisabarro, M. T., and Serrano, L. (1996) *Biochemistry 35*, 10634−10640.
39. Briggs, S. D., Lerner, E. C., and Smithgall, T. E. (2000) *Biochemistry 39*, 489−495.
40. Saksela, K., Cheng, G., and Baltimore, D. (1995) *EMBO J. 14*, 484−491.

BI020475Y